DOI: 10.13009/EUCASS2017-255

7TH EUROPEAN CONFERENCE FOR AERONAUTICS AND AEROSPACE SCIENCES (EUCASS)

DOI: ADD DOINUMBER HERE

Numerical simulation of the flow around a flapping-wing micro air vehicle in free flight

Moriche M.†*, Hernández-Hurtado E., Flores O and García-Villalba M.*
Universidad Carlos III de Madrid
Address
mmoriche@ing.uc3m.es
†Corresponding author

Abstract

We present direct numerical simulations of the flow around a simplified model of a flapping-wing micro air vehicle in uncontrolled forward flight at low Reynolds number, including the vehicle dynamics. A simple model for the vehicle is employed, including wings, tail and fuselage. Only a symmetric flight condition will be discussed. The wing kinematics are externally imposed and the vehicle moves as a result of the aerodynamic forces and gravity. The simulations are initialized by keeping the vehicle fixed in space in the presence of a free-stream of constant speed, flapping the wings for several periods. The gravity is adjusted using the average lift during this initial transient, after which the vehicle is released. We analyze the initial stages after the release of the vehicle, placing emphasis on how the aerodynamic forces and the flow around the vehicle are modified once the vehicle is released.

1. Introduction

There is a growing interest in the development of very small unmanned air vehicles, so called micro air vehicles (MAVs). Efficient designs of fixed and rotary wing MAVs have been already attained, but flapping wing MAVs are still on its early stages of the development process. Flapping wing MAVs have the potential of high maneuverability, indoor flight capabilities and more silent performance than fixed or rotary wing MAVs. The operating conditions in which these devices operate is similar to those in which small birds and insects fly, so that by bio-mimicking these species we hope to achieve their outstanding flight capabilites.[9]

The controlled flight of a MAV is a complex multidisciplinary problem as sketched in figure 1, involving unsteady aerodynamics, flight mechanics, control theory and structural analysis, among others. There is a complex interaction between the various sub-problems, increasing even more the complexity of the whole problem.

Different studies in the literature have adopted different approaches to learn from the problem of flapping wing flight. Recent reviews are provided by Taha et al.,[12] Orlowski and Girard[7] and Sun.[10] Concerning flow stability, Sun and Xiong[11] studied the stability of a model of a bumblebee. They found that there are stable and unstable flight modes, so the uncontrolled flight of this specie is unstable. Nevertheless, the time required to increase by a factor of two the perturbation intensity is around 15 times the beating period, so the bumblebee has enough time to modify the kinematics and, therefore, reach controlled flight. Minami et al.[3] studied both uncontrolled and controlled flight of a Dragonfly model at a Re based on the maximum wing velocity of $Re = 200$. They varied the lag between the motion of the forewing and the hindwing, ϕ. Independently of the value of ϕ the dragonfly flights forward, whereas depending on the value of ϕ, the dragonfly can move up, down or horizontally. Without control, the flight is unstable, so that they introduced a small modification in the kinematics of the forewing as a control strategy, obtaning satisfactory results. In a different study, Nakatani et al.[6] evaluated different strategies to control the flight of a butterfly model. They used a moving weight to control the pitching and rolling motions with P and PI control schemes, respectively. They also performed control of the pitching motion by modifying the kinematics of the vehicle (interrupting the motion in specific instants) with a PID control scheme. More recently, Deng et al.[1] recorded the wing deformations of an actual flapping wing MAV and, then, imposed these deformations as prescribed kinematics in a numerical model.

In this work, we present a computational model of the uncontrolled forward flight of a simplified model of a flapping wing MAV. To this aim, three aspects need to be considered, namely, wing kinematics, the resulting aerodynamic forces due to the flapping motion and finally the motion of the MAV as a result of the aerodynamic forces and its own weight. The wing kinematics are externally imposed. The aerodynamic forces are calculated by means of

DOI: 10.13009/EUCASS2017-255

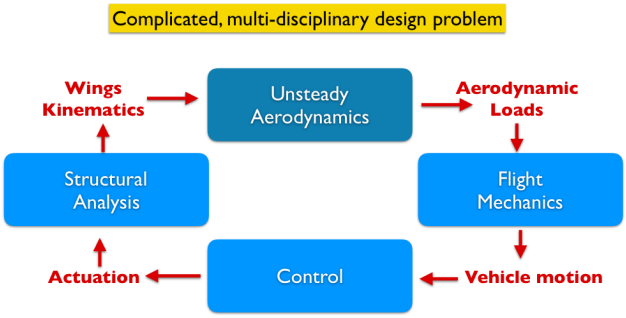

Figure 1: Disciplines involved in the controlled flight of a flapping-wing MAV, adapted from Taha et al.[12]

Direct Numerical Simulation (DNS) of the incompressible flow surrounding the MAV. Finally, the motion of the MAV is obtained by solving the Newton-Euler equations for the MAV. These two sets of equations are coupled as discussed below.

2. Methodology

The governing equations are integrated numerically with TUCAN,[4,5] an extensively validated solver to simulate the flow around moving bodies of arbitray shape. TUCAN solves the Navier Stokes equations for an incompressible flow

$$\frac{\partial u_i}{\partial x_i} = 0, \tag{1a}$$

$$\frac{\partial u_i}{\partial t} + u_j \frac{\partial u_i}{\partial x_j} = -\frac{1}{\rho_f}\frac{\partial p}{\partial x_i} + \nu \frac{\partial^2 u_i}{\partial x_i^2}, \tag{1b}$$

$$B(u_i) = 0 \quad \text{at domain boundaries}, \tag{1c}$$

$$u_i = U_i \quad \text{at body surface}, \tag{1d}$$

where u_i is the flow velocity, p is the pressure, ν and ρ_f are the kinematic viscosity and density of the fluid, respectively, U_i is the velocity of the body at the surface of the body and $B(u_i)$ represents the boundary conditions at the domain boundaries. Spatial discretization is done with second order centered finite differences on a structured, uniform Cartesian grid and time marching is performed with a three stages semi-implicit Runge-Kutta scheme. The presence of the body is modelled with the direct forcing immersed boundary method proposed by Uhlmann.[14] Regarding the equations of motion, the algorithm presented in the work of Uhlmann is only valid for spherical bodies. In order to avoid this constraint, we have implemented an algorithm in which the rotation of the body and the inertia properties of bodies of arbitrary shape are taken into account. The equations of motion read

$$\rho_b V_b \frac{\mathrm{d}\vec{u}_\mathrm{G}}{\mathrm{d}t} = \rho_f \oint_S \bar{\tau}\cdot\vec{n}\,\mathrm{d}S, \tag{2a}$$

$$\frac{\mathrm{d}\vec{H}_\mathrm{G}}{\mathrm{d}t} = \rho_f \oint_S \vec{r}\times(\bar{\tau}\cdot\vec{n})\,\mathrm{d}S, \tag{2b}$$

where $\vec{u}_\mathrm{G}$ is the velocity of the center of gravity, V_b is the volume of the body, $\bar{\tau}$ is the stress tensor, $\vec{n}$ is a unitary normal vector pointing towards the fluid and S represents the domain that the body occupies. The right hand side of equation 2 can be expanded as

$$\rho_f \oint_S \bar{\tau}\cdot\vec{n}\,\mathrm{d}S = -\rho_f \int_S \vec{f}\,\mathrm{d}\vec{x} + \rho_f \frac{\mathrm{d}}{\mathrm{d}t}\int_S \vec{u}\,\mathrm{d}\vec{x} = -\rho_f \int_S \vec{f}\,\mathrm{d}\vec{x} + \rho_f V_b \frac{\mathrm{d}\vec{u}_\mathrm{G}}{\mathrm{d}t}, \tag{3a}$$

$$\rho_f \oint_S \vec{r}\times(\bar{\tau}\cdot\vec{n})\,\mathrm{d}S = -\rho_f \int_S \vec{r}\times\vec{f}\,\mathrm{d}\vec{x} + \rho_f \frac{\mathrm{d}}{\mathrm{d}t}\int_S \vec{r}\times\vec{u}\,\mathrm{d}\vec{x} = -\rho_f \int_S \vec{r}\times\vec{f}\,\mathrm{d}\vec{x} + \frac{\rho_f}{\rho_b}\frac{\mathrm{d}\vec{H}_\mathrm{G}}{\mathrm{d}t}, \tag{3b}$$

DOI: 10.13009/EUCASS2017-255

where $\vec{f}$ is the fluid-solid coupling force which can be easily computed in the context of the present immersed boundary method, for the details see Uhlmann.[14] Substituting 3 in 2 leads to

$$\frac{\mathrm{d}\vec{u}_\mathrm{G}}{\mathrm{d}t} = \frac{-1}{V_b\left(\rho_b/\rho_f - 1\right)} \int_S \vec{f}\mathrm{d}\vec{x}, \tag{4a}$$

$$\frac{\mathrm{d}\vec{H}_\mathrm{G}}{\mathrm{d}t} = \frac{-\rho_f}{1-\rho_f/\rho_b} \int \vec{r}\times\vec{f}\mathrm{d}\vec{x}. \tag{4b}$$

In order to solve eq. 4b, it is convenient to consider a body-fixed reference frame aligned with the principal axes of the body. Then, the components of the time derivative of the angular momentum read

$$\frac{\mathrm{d}\vec{H}_\mathrm{G}}{\mathrm{d}t} \cdot \vec{e}_x = I_x\dot{p} - \left(I_y - I_z\right)rq, \tag{5a}$$

$$\frac{\mathrm{d}\vec{H}_\mathrm{G}}{\mathrm{d}t} \cdot \vec{e}_y = I_y\dot{r} - \left(I_z - I_x\right)qp, \tag{5b}$$

$$\frac{\mathrm{d}\vec{H}_\mathrm{G}}{\mathrm{d}t} \cdot \vec{e}_z = I_z\dot{q} - \left(I_x - I_y\right)pr, \tag{5c}$$

where I_x, I_y and I_z are the moments of inertia in the principal axes of the body in the x, y and z directions, respectively, and p, r and q are the components of the angular velocity $\vec{\Omega} = (p, r, q)$. Furthermore, we have used quaternions $\vec{q}$ to track the rotation of the body in order to eliminate the singularities that appear with Euler angles. The quaternions $\vec{q}$ define a rotation with the direction of the axis of rotation $\vec{e} = (e_1, e_2, e_3)$ and the angle rotated φ. The evolution in time of $\vec{q}$ is given by

$$\frac{\mathrm{d}\vec{q}}{\mathrm{d}t} = \frac{1}{2}\bar{Q}\vec{q}, \tag{6}$$

where $q_i = e_i \sin(\varphi/2)$ for $i = 1, 2, 3$ and $q_4 = \cos(\varphi/2)$ and

$$\bar{Q} = \begin{pmatrix} 0 & q & -r & p \\ -q & 0 & p & r \\ r & -p & 0 & q \\ -p & -r & -q & 0 \end{pmatrix}. \tag{7}$$

2.1 Vehicle

The MAV consists of a fuselage or body, two wings and, in some cases, a tail. The wings and the tail are considered massless, so the inertia of the MAV is the inertia of the body. The density of the body ρ_b is set to $\rho_b/\rho_f = 1000$, where ρ_f is the density of the fluid.

The body is modelled as a prolate spheroid whose long and short dimensions are L and w, respectively. The selection of the Aspect Ratio (AR) of the body $\mathrm{AR}_b = L/w$ is based on work found in the literature about flying species in nature. Insects have slender bodies, but also they are articulated, so in order to reduce the complexity of the model, we focus our attention in hummingbirds. The AR_b of hummingbirds takes values in the range of $\mathrm{AR}_b = 3 - 5$.[13] We have selected a value of $\mathrm{AR}_b = 3$ in our simulations. Wings are modelled following the work or Pedersen,[8] in which the combination of four ellipses results in a wing geometry similar to that found in insects (see figure 2). Each wing is defined by its span, b, and maximum chord, c. According to the work of Tobalske et al.[13] and Kruyt et al.,[2] the AR of wings $\mathrm{AR}_w = b/c$ takes values in the range of $\mathrm{AR}_w = 3 - 4$. We select a value of $\mathrm{AR}_w = 3.8$ in our simulations. Another important geometry parameter is the distance from the root of the wings to the center of gravity, d_r. According to Wu et al.,[15] the root of the wings should be placed ahead of the center of gravity of the body, with values in the range of $d_r/L = 0.13 - 0.26$. We have located the root of the wings ahead of the center of gravity at a distance $d_r/L = 0.14$ from it. Finally, a tail is included in one of the cases under study. The tail is an elliptic wing with maximum chord c_t and aspect ratio AR_t equal to the values of the wing c and AR_w, respectively.

2.2 Wing Kinematics

The kinematics of the wings is a combination of flapping (ϕ) and pitching (α) motions (see figure 3). The former, flapping, is the motion in which the spanwise axis of the wing rotates inside the stroke plane. The pivoting point of the flapping motion of each wing is its root. Note that the stroke plane is always perpendicular to the long axis of the body.

DOI: 10.13009/EUCASS2017-255

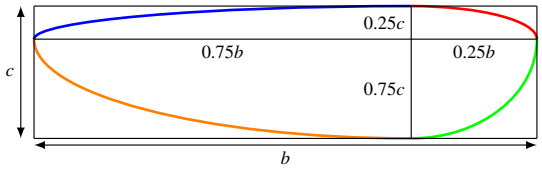

Figure 2: Model of wing with four ellipses (see Pedersen et al.[8]).

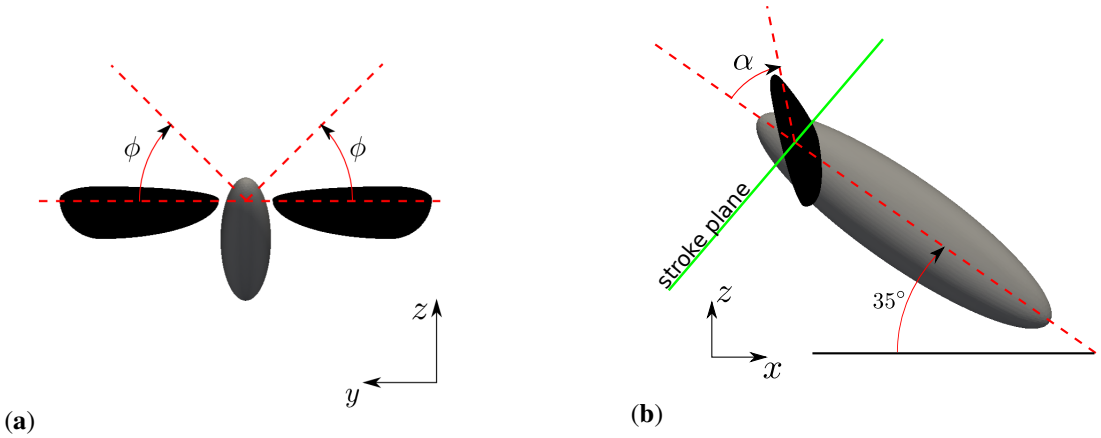

Figure 3: Outline of the kinematics imposed on the vehicle.

The pitching motion is the rotation of the wing around its spanwise axis. Flapping and pitching motions are described with sinusoidal laws

$$\phi = \phi_0 \cos(2\pi f), \tag{8}$$

$$\alpha = \alpha_0 \cos(2\pi f + \varphi), \tag{9}$$

where ϕ_0 and α_0 are the flapping and pitching amplitudes, respectively, f is the frequency of oscillation and φ the phase shift between both motions. In this work we have selected a reduced frequency of $k = 2\pi f c/U_\infty = 1$, where U_∞ is the free stream velocity. The amplitude of the motion is set to $\phi_0 = 60°$ and $\alpha_0 = 45°$ for the flapping and pitching motion, respectively. Finally, the phase shift between both motions is $\varphi = 90°$.

2.3 Computational setup

The problem under study consists in an flapping wing MAV submerged in a free stream of velocity U_∞. The Re of the flow based on the free stream velocity and the maximum chord is $\mathrm{Re}_\infty = U_\infty c/\nu = 250$. If the maximum velocity of the wing tip U_{TIP} is used as a reference magnitude the Re is approximately $\mathrm{Re}_{\mathrm{TIP}} = U_{\mathrm{TIP}} c/\nu \approx 1000$. The computational domain is [20c x 20c x 10c] in the streamwise (x), spanwise (y) and vertical (z) directions, respectively, discretized with [512 x 512 x 256] points in each direction. This yields a resolution of approximately $c/\Delta x \approx 25$ points per maximum chord c. The boundary conditions imposed are inflow/outflow in the streamwise direction and periodic in the spanwise and vertical directions. The MAV is placed in the middle of the domain, with its long axis oriented parallel to a plane xz and with an angle of 35° with a plane xy (see figure 3b). Finally, the time step Δt is selected to have a maximum Courant Friedrich Levy (CFL) number of 0.45.

Regarding the set of cases presented here, we start from a reference case in which no motion is allowed to the body of the MAV, except for the prescribed kinematics of the wings. Also, this case has no tail. We refer to this case as “Pinned”. The second case, referred as “Free”, has no constraints in the motion of the body of the MAV and, also, has no tail. The motion of the body of the MAV is determined by the equations of motions and the motion of the wings is prescribed relative to the body. The third case, referred as “Free T”, is similar to the previous one, except for the inclusion of a tail in its geometry. We use the tail as a possible strategy to obtain stable flight.

DOI: 10.13009/EUCASS2017-255

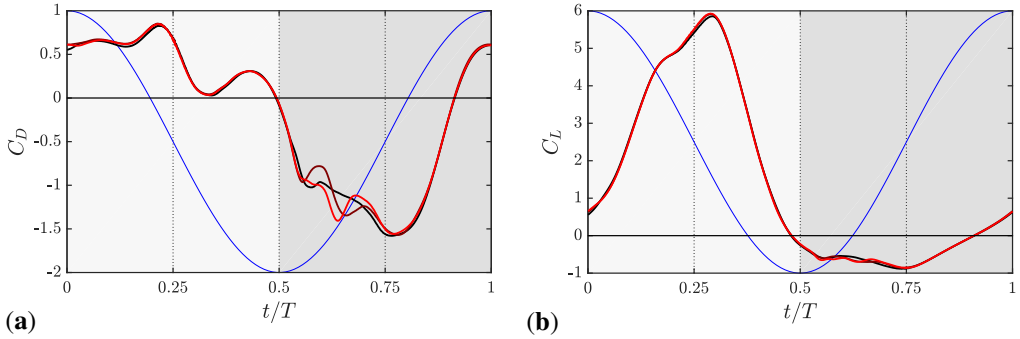

Figure 4: a) Drag and b) Lift coefficients obtained in case Pinned. Cycle 1 ( ), cycle 2 ( ) and cycle 3 ( ) are represented together with the stroke angle ϕ ( ) for reference. The downstroke (upstroke) is represented in light (dark) grey.

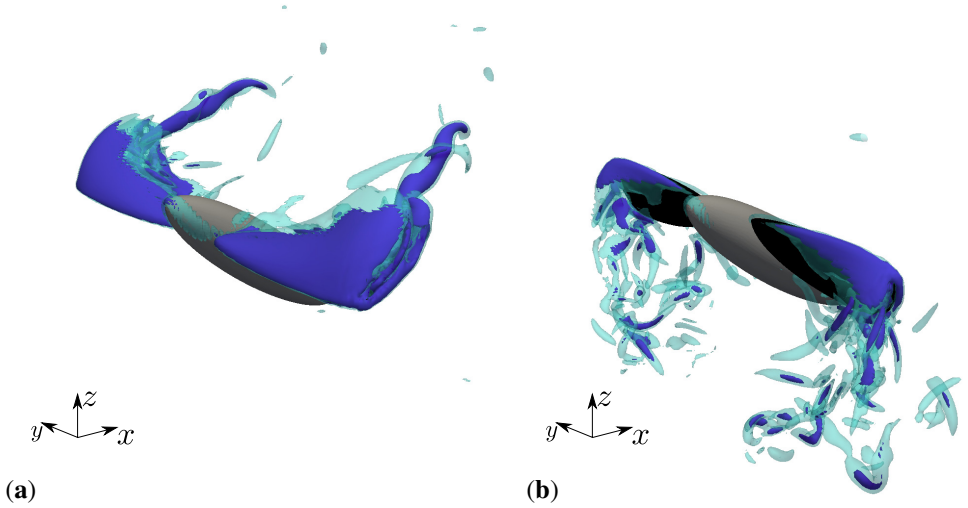

Figure 5: Iso-surfaces of Q criterion for case Pinned at middle of a) downstroke and b) upstroke.

3. Results

In this section we analyze the aerodynamic forces and flow structures that appear in the different cases. We also study the motion of the MAV when the vehicle is released (cases "Free" and "Free T").

We start analyzing case "Pinned". This case has no tail and the position of the body is fixed. Figure 4 shows that the aerodynamic forces obtained converge to a periodic state. During the downstroke ($0 < t/T < 0.5$), high lift is generated (figure 4b) at the expense of generating drag (figure 4a). Conversely, thrust and negative lift are generated during the upstroke ($0.5 < t/T < 1$).

Figure 5 shows the flow around the MAV for case "Pinned" by means of iso-surfaces of the Q criterion. The Leading Edge Vortex (LEV) is generated on the upper and lower surface in the downstroke and upstroke, respectively. Each section of the wing travels at a speed of $r\dot{\phi}$, where r is the distance of each section to the wing root. Because the MAV is in a free stream, the velocity seen by each section of the wing is the combination of $r\dot{\phi}$ in the direction of the stroke and the free stream velocity $U_\infty \vec{e}_x$, where $\vec{e}_x$ is a unitary vector in the x (streamwise) direction. This results in a higher velocity seen by the airfoil during the downstroke than during the upstroke, resulting in a larger LEV in the former than in the latter. Furthermore, the Tip Vortex (TiV) generated in the downstroke remains coherent whereas the generated in the upstroke are broken by the free stream.

If the Micro Air Vehicle (MAV) is released (case "Free"), the evolution of the aerodynamic forces deviates from the periodic state reached in the case "Pinned". Figure 6 shows the aerodynamic forces, moment and orientation of the vehicle for case "Free". Figure 6a shows that the drag generated during the downstroke grows from one cycle to

DOI: 10.13009/EUCASS2017-255

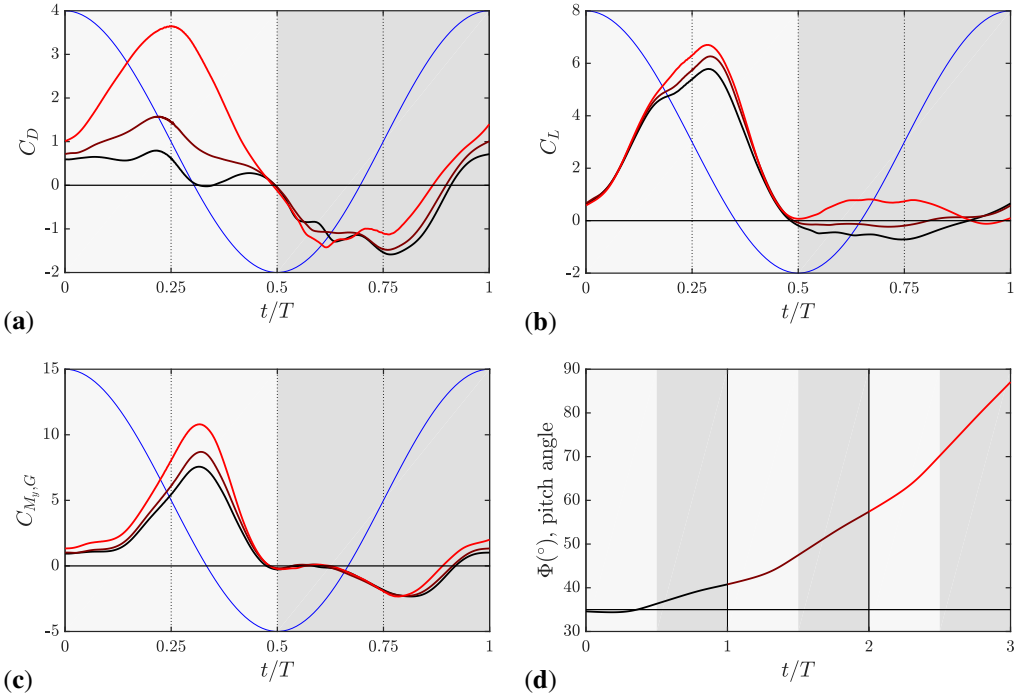

Figure 6: a) Drag and b) Lift coefficients obtained in case Free. Cycle 1 ( ), cycle 2 ( ) and cycle 3 ( ) are represented together with the stroke angle ϕ ( ) for reference. The downstroke (upstroke) is represented in light (dark) grey.

the next one, whereas the thrust generated during the upstroke remains similar. Regarding the lift generated during the downstroke, it starts growing and then decreases, whereas the lift generated during the upstroke grows monotonically from cycle to cycle (figure 6b). The spanwise moment about the center of gravity grows during the whole period as the cycles evolve (figure 6c), resulting in an uncontrolled nose up motion of the MAV (figure 6d).

Figure 7 shows the flow around the MAV for case "Free" at the middle of the upstroke for two different cycles. One cycle after being released (figure 7a), the vehicle still keeps an orientation similar to the initial one and the flow around the vehicle is similar as in the case "Pinned" (figure 5b). Two cycles after being released (figure 7b), the vehicle has rotated around its spanwise axis more than 30°, so the body long axis its oriented almost vertically. The differences observed in the forces in figure 6 is influenced by the different orientation of the MAV and a much incoherent flow structures around the wings (figure 7b).

The main issue encountered when the vehicle is released is a non-compensated moment around the spanwise axis. The first and, maybe, the most simple, device that one could use to damp this non-compensated moment is a tail. Figure 7a shows a comparison of the aerodynamic spanwise moment around the center of gravity generated in the case "Free" (no tail) and case "FreeT" (tail). There is a noticeable reduction of the pitch-up moment when the tail is incorporated. This results in a reduction of the pitch angle of the body (figure 7b) to almost one half of the value obtained in the case without tail. Therefore, considering its simplicity, the presence of a tail shows as a good strategy to compensate the nose-up motion of the free flight of the vehicle.

4. Conclusions

We have presented proof-of-concept DNS of a flapping wing MAV in uncontrolled forward flight. The calculations have been performed with the in-house code TUCAN, a solver in which the solution of Navier Stokes equation is coupled with the Newton-Euler equations of the rigid body to determine the motion of the MAV. A case in which the body is fixed is used as a reference to analyze the motion of the MAV when it is released. In all the cases the flight is trimmed in forces, but not in moments. Therefore a nose up maneuver dominates the subsequent motion of the MAV. This nose up results in a large modification of the aerodynamic forces and a modification of the flow structures around the wings. As a first try to compensate for the large spanwise moment generated, we have included a tail in our model of the MAV. With this approach, the spanwise moments are noticeably reduced during the whole period. As a result,

DOI: 10.13009/EUCASS2017-255

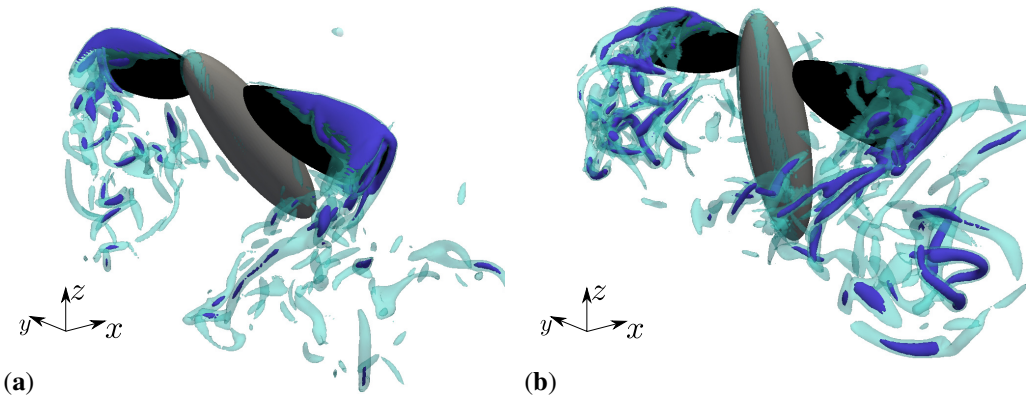

Figure 7: Flow visualization of Q criterion for case Free at middle of upstroke after a) 1 period from its release and b) 2 periods from its release.

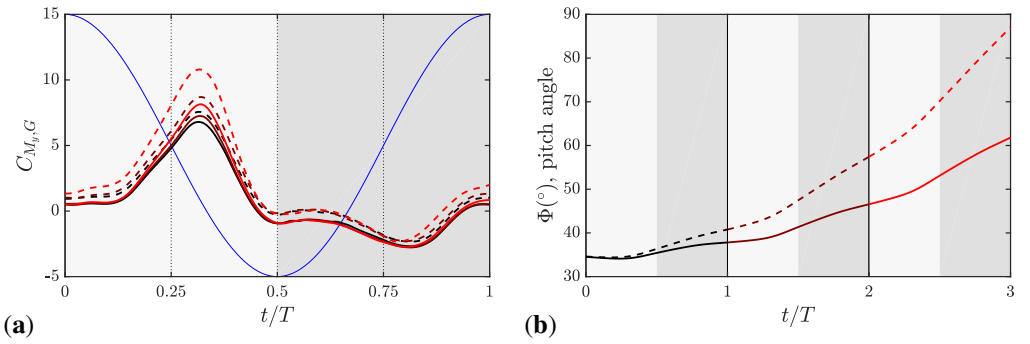

Figure 8: a) Spanwise moment with respect to the center of gravity and d) pitch angle of the vehicle obtained in case Free. Cycle 1 ( ), cycle 2 ( ) and cycle 3 ( ) are represented together with the stroke angle ϕ ( ) for reference. For comparison purposes, the results of case Free are included in the figure with dashed lines. The downstroke (upstroke) is represented in light (dark) grey.

DOI: 10.13009/EUCASS2017-255

the pitching of the MAV is reduced in almost one half of the value of the pitching of the case without tail.

5. Acknowledgments

This work was supported by grant TRA2013-41103-P of the Spanish Ministry of Economy and Competitiveness. This grant includes FEDER funding. MGV was partially supported by a grant of the BBVA Foundation.

References

[1] S. Deng, M. Percin, B. W. van Oudheusden, H. Bijl, B. Remes, and T. Xiao. Numerical simulation of a flexible X-wing flapping-wing micro air vehicle. *AIAA*, 0:1–12, 2017.

[2] J. W. Kruyt, E. M. Quicazán-Rubio, G. F. van Heijst, D. L. Altshuler, and D. Lentink. Hummingbird wing efficacy depends on aspect ratio and compares with helicopter rotors. *J. R. Soc. Interface*, 11(99):20140585, 2014.

[3] K. Minami, K. Suzuki, and T. Inamuro. Free flight simulations of a dragonfly-like flapping wing-body model using the immersed boundary-lattice boltzmann method. *Fluid Dyn. Res.*, 47(1):015505, 2014.

[4] M. Moriche. *A numerical study on the aerodynamic forces and the wake stability of flapping flight at low Reynolds number*. PhD thesis, Universidad Carlos III de Madrid, 2017.

[5] M. Moriche, O. Flores, and M. García-Villalba. Three-dimensional instabilities in the wake of a flapping wing at low Reynolds number. *Int. J. Heat Fluid Flow*, 62:44–55, 2016.

[6] Y. Nakatani, K. Suzuki, and T. Inamuro. Flight control simulations of a butterfly-like flapping wing–body model by the immersed boundary–lattice boltzmann method. *Comput. Fluids*, 133:103–115, 2016.

[7] C. T. Orlowski and A. R. Girard. Modeling and simulation of nonlinear dynamics of flapping wing micro air vehicles. *AIAA J.*, 49(5):969–981, 2011.

[8] C. B. Pedersen. *An indicial-Polhamus model of aerodynamics of insect-like flapping wings in hover*. PhD thesis, Cranfield University, 2011.

[9] W. Shyy, H. Aono, C.-K. Kang, and H. Liu. *An introduction to flapping wing aerodynamics*. Cambridge Univ. Press, 2013.

[10] M. Sun. Insect flight dynamics: stability and control. *Rev. Mod. Phys.*, 86(2):615, 2014.

[11] M. Sun and Y. Xiong. Dynamic flight stability of a hovering bumblebee. *J. Exp. Biol.*, 208(3):447–459, 2005.

[12] H. E. Taha, M. R. Hajj, and A. H. Nayfeh. Flight dynamics and control of flapping-wing mavs: a review. *Nonlinear Dyn.*, 70(2):907–939, 2012.

[13] B. W. Tobalske, D. R. Warrick, C. J. Clark, D. R. Powers, T. L. Hedrick, G. A. Hyder, and A. A. Biewener. Three-dimensional kinematics of hummingbird flight. *J. Exp. Biol.*, 210(13):2368–2382, 2007.

[14] M. Uhlmann. An immersed boundary method with direct forcing for the simulation of particulate flows. *J. Comp. Phys.*, 209(2):448–476, 2005.

[15] J. H. Wu, Y. L. Zhang, and M. Sun. Hovering of model insects: simulation by coupling equations of motion with navier–stokes equations. *J. Exp. Biol.*, 212(20):3313–3329, 2009.